



Cite this: *Phys. Chem. Chem. Phys.*, 2018, 20, 25009

High-symmetry tubular Ta@B₁₈³⁻, Ta₂@B₁₈, and Ta₂@B₂₇⁺ as embryos of α -boronanotubes with a transition-metal wire coordinated inside†

Hai-Ru Li, Hui Liu, Xiao-Yun Zhao, Ling Pei, Na Chen, Wen-Yan Zan, Hai-Gang Lu, Yue-Kui Wang, Yue-Wen Mu * and Si-Dian Li *

Transition-metal doping leads to dramatic structural changes and results in novel bonding patterns in small boron clusters. Based on the experimentally derived mono-ring planar C_{9v} Ta@B₉²⁻ (**1**) and extensive first-principles theory calculations, we present herein the possibility of high-symmetry double-ring tubular D_{9d} Ta@B₁₈³⁻ (**2**) and C_{9v} Ta₂@B₁₈ (**3**) and triple-ring tubular D_{9h} Ta₂@B₂₇⁺ (**4**), which may serve as embryos of single-walled metalloboronanotube α -Ta₃@B_{48(3,0)} (**5**) wrapped up from the recently observed most stable free-standing boron α -sheet on a Ag(111) substrate with a transition-metal wire (-Ta-Ta-) coordinated inside. Detailed bonding analyses indicate that, with an effective d_{z²}-d_{z²} overlap on the Ta-Ta dimer along the C₉ molecular axis, both Ta₂@B₁₈ (**3**) and Ta₂@B₂₇⁺ (**4**) follow the universal bonding pattern of $\sigma + \pi$ double delocalization with each Ta center conforming to the 18-electron rule, providing tubular aromaticity to these Ta-doped boron complexes with magnetically induced ring currents. The IR, Raman, and UV-vis spectra of **3** and **4** are computationally simulated to facilitate their future experimental characterization.

Received 20th July 2018,
Accepted 7th September 2018

DOI: 10.1039/c8cp04602f

rs.li/pccp

1. Introduction

As a prototypic electron-deficient element dominated by multicenter-two-electron (mc-2e) bonding in both bulk allotropes and polyhedron molecules, boron has a rich chemistry next only to carbon in the periodical table.¹⁻⁴ Over ten years of persistent joint photoelectron spectroscopy (PES) and first-principles theory investigations on small boron monoanions have revealed a rich landscape from planar or quasi-planar B_n^{-/0} (n = 3-30, 33-38) to cage-like borospherenes D_{2d}B₄₀^{-/0} and C₃/C₂B₃₉⁻.³⁻¹⁰ The borospherene family has been systematically expanded at first-principles theory levels in recent years to include the cage-like B_n^q series (n = 36-42, q = n-40).¹¹⁻¹⁴ Ion-mobility measurements in combination with density functional theory (DFT) calculations, on the other hand, have shown that B_n⁺ monocations (n = 16-25) possess double-ring tubular (DRT) structures, unveiling another important structural domain in boron chemistry.¹⁵ Although both single-walled and multi-walled boron nanotubes have been observed in experiments, no atomic structures of such boron nanotubes have been determined to date.^{16,17} Various boron nanotubes wrapped up from the most stable free-standing boron α -sheet with a

hole-density of $\eta = 1/9^{18-20}$ and a snub-sheet with $\eta = 1/8^{21}$ have been predicted at the DFT level, but none of them have been confirmed in experiments. Joint experimental and theoretical investigations have indicated that the incorporation of a transition-metal (M) dopant leads to dramatic structural changes and results in novel bonding patterns in small boron clusters, as shown in the cases of the perfect mono-ring planar (MRP) D_{8h} Co@B₈⁻, D_{9h} Ru@B₉⁻, and D_{10h} Ta@B₁₀⁻ and double-ring tubular D_{8d} Co@B₁₆⁻, D_{9d} Rh@B₁₈⁻, and D_{10d} Ta@B₂₀⁻ mononuclear complexes,²²⁻²⁵ which set the highest possible coordination numbers to CN = 10 in planar and CN = 20 in tubular environments *via* effective M-B_n coordination interactions, respectively. Based on the typical fluctuation behaviour of the Ni-doped half-sandwich C_{2v} NiB₁₁⁻, our group recently proposed the concept of fluxional bonds in chemistry.²⁶ We also predicted a series of mononuclear endohedral metalloborospherenes, Ta@B_n^q (n = 22-28, q = -1 to +3), as superatoms in 18-electron configurations, unveiling the tubular-to-cage-like structural transition at endohedral cage-like D₂ Ta@B₂₂⁻ and the highest coordination number of CN_{max} = 28 in spherical environments.^{27,28} A slightly distorted MRP C_s Ta@B₉⁻ was recently observed in PES experiments due to the Jahn-Teller effect, with perfect singlet MRP C_{9v} Ta@B₉²⁻ and triplet C_{9v} Ta@B₉ derived from the monoanion.²⁹ A DRT C₂ Ta@B₁₈⁻ was recently proposed in theory.³⁰ Endohedral M@B₄₀ (M = Ca, Sr)³¹ and penta-ring tubular Ca@B₅₆ charge-transfer complexes³²

Institute of Molecular Science, Shanxi University, Taiyuan, 034000, China.

E-mail: ywmu@sxu.edu.cn, lisidian@sxu.edu.cn

† Electronic supplementary information (ESI) available. See DOI: 10.1039/c8cp04602f

have also been predicted. Small dinuclear $\text{Ta}_2\text{B}_n^{-/0}$ clusters ($n = 2-5$) observed in PES measurements possess incomplete bipyramid structures with an equatorial boron belt around a Ta-Ta dimer.³³ Ni-doped exohedral heteroborosphenes $\text{Ni}_n \in \text{B}_{40}$ ($n = 1-4$) with 1-4 heptacoordinate Ni centers have been predicted by first-principles theory.³⁴ However, to the best of our knowledge, there have been no theoretical or experimental investigations reported to date on di- or multi-nuclear double-ring tubular, triple-ring tubular (TRT), or multi-ring tubular (MRT) boron complexes with a transition-metal dimer (M-M) or wire (-M-M-) coordinated inside.

Based upon the experimentally derived MRP $C_{9v} \text{Ta} \odot \text{B}_9^{2-}$ (1) and extensive global minimum searches and first-principles theory calculations, we predict herein the possible existence of mono-nuclear DRT $D_{9d} \text{Ta} @ \text{B}_{18}^{3-}$ (2) and dinuclear DRT $C_{9v} \text{Ta}_2 @ \text{B}_{18}$ (3) and TRT $D_{9h} \text{Ta}_2 @ \text{B}_{27}^+$ (4), which may serve as embryos of single-walled metalloboronanotube $\alpha\text{-Ta}_3 @ \text{B}_{48(3,0)}$ (5) with a transition-metal wire (-Ta-Ta-) coordinated inside.¹⁸⁻²⁰ Both $\text{Ta}_2 @ \text{B}_{18}$ (3) and $\text{Ta}_2 @ \text{B}_{27}^+$ (4) are effectively stabilized *via* spd- π coordination interactions between the Ta-Ta dimer and B_n ligands ($n = 18$ and 27), which match both geometrically and electronically. Such tubular aromatic dinuclear complexes follow the universal bonding pattern of $\sigma + \pi$ double delocalization with each Ta center conforming to the 18-electron rule.

2. Theoretical procedure

Extensive global minimum searches were performed on TaB_{18}^{3-} , Ta_2B_{18} , and $\text{Ta}_2\text{B}_{27}^+$ using both the Minima Hopping algorithm^{35,36} and TGmin code³⁷ at the DFT level, in combination with manual structural constructions based on the previously reported $\text{B}_n^{-/0/+}$ clusters ($n = 18, 27$).³⁻¹⁰ More than 3000 stationary points were explored for each system at the PBE/DZVP level. Low-lying isomers were then fully optimized at the PBE0,³⁸ TPSSH,³⁹ and HSE06⁴⁰ levels with the 6-311+G* basis set⁴¹ for B and Stuttgart relativistic small-core pseudopotential for Ta, Hf, Zr, W, and Nb^{42,43} using the Gaussian 09 program suite,⁴⁴ with vibrational frequencies calculated using the harmonic approximation to make sure that the optimized structures are true minima of the systems. The convergence criterion for total energy was set to be 10^{-10} Hartree/particle and tight thresholds were employed for geometry optimizations in Gaussian 09.⁴⁴ For the five lowest-lying isomers of TaB_{18}^{3-} within 1.43 eV and Ta_2B_{18} within 1.09 eV at the PBE0 level, we performed single-point calculations at the more accurate CCSD(T)⁴⁵⁻⁴⁷ level (within 1.22 and 2.06 eV, respectively, Fig. S1 and S2, ESI[†]) using the MOLPRO 2013 package.⁴⁸ Chemical bonding analyses were performed using the adaptive natural density partitioning (AdNDP) method⁴⁹ at the PBE0/6-31G level of theory to recover both the localized and delocalized bonding interactions in the systems. The magnetically induced ring current maps of 1-4 were generated using the anisotropy of the current-induced density (ACID) approach.^{50,51} The UV-vis spectra of the relevant clusters were simulated using the time-dependent TD-DFT approach⁵² at the PBE0 level. Natural bonding analyses were performed using the NBO 6.0 program.⁵³

The Ta-doped one-dimensional (1D) metalloboronanotube $\alpha\text{-Ta}_3 @ \text{B}_{48(3,0)}$ (5) constructed by rolling up the most stable free-standing boron α -sheet in the (3,0) direction was optimized using the Vienna ab initio simulation package (VASP)^{54,55} at the Perdew-Burke-Ernzerhof (PBE)⁵⁶ level with the projector augmented wave (PAW)^{57,58} pseudopotential method.

3. Results and discussion

3.1 Structures and stabilities

We start from the perfect singlet DRT $D_{9d} \text{Ta} \odot \text{B}_{18}^{3-}$ (2) with two staggered B_9 rings in a $D_{9d} \text{B}_{18}$ ligand (Fig. 1), which can be constructed by capping a $D_{9h} \text{B}_9$ mono-ring atop the experimentally derived singlet MRP $C_{9v} \text{Ta} \odot \text{B}_9^{2-}$ (1) or its neutral triplet counterpart $C_{9v} \text{Ta} \odot \text{B}_9^{30}$ with an optimized diameter of $d = 4.66 \text{ \AA}$ and a Ta-B coordination bond length of $r_{\text{Ta-B}} = 2.48 \text{ \AA}$. It can also be obtained by attaching two extra electrons to the slightly distorted DRT $C_2 \text{Ta} @ \text{B}_{18}^-$ previously predicted in theory³⁰ with the extra electrons located in two degenerate HOMOs. With a HOMO-LUMO energy gap of $\Delta E_{\text{gap}} = 0.82 \text{ eV}$ and a smallest vibrational frequency of $\nu_{\text{min}} = 131 \text{ cm}^{-1}$ at PBE0, $\text{Ta} @ \text{B}_{18}^{3-}$ (2) is the well-defined global minimum (GM) of the system, 1.22 and 1.02 eV more stable than the second basket-like isomer $C_s \text{Ta} @ \text{B}_{18}^{3-}$ at the PBE0 and CCSD(T) levels, respectively (Fig. S1a and S2a, ESI[†]). Tubular $\text{Ta} @ \text{B}_{18}^{3-}$ (2) achieves the highest symmetry of D_{9d} of the system, similar to the experimentally observed $D_{10d} \text{Ta} @ \text{B}_{20}^-$.²⁵ Its Ta center possesses the natural atomic charge of $q_{\text{Ta}} = +0.50 |e|$, electronic configuration of $\text{Ta}[\text{Xe}]5d^{4.11}6s^{0.19}$, total Wiberger bond order of $\text{WBI}_{\text{Ta}} = 5.11$, and Ta-B coordination bond order of $\text{WBI}_{\text{Ta-B}} = 0.29$ (Table S1, ESI[†]). Incorporation of a Ca^{2+} dication into $\text{Ta} @ \text{B}_{18}^{3-}$ (2) effectively stabilizes the trianion and generates a highly stable $C_{9v} \text{Ca}[(\text{Ta} @ \text{B}_{18})]^-$ monoanion with $\Delta E_{\text{gap}} = 2.88 \text{ eV}$ and $\nu_{\text{min}} = 160 \text{ cm}^{-1}$, similar to dinuclear $C_{9v} \text{Ta}_2 @ \text{B}_{18}$ (3) discussed in detail in the following section.

Adding one more Ta atom atop $\text{Ta} @ \text{B}_{18}^{3-}$ (2) along the C_9 molecular axis results in the Ta-capped nonagonal antiprism $C_{9v} \text{Ta}_2 @ \text{B}_{18}$ (3) (Fig. S1b and S2b, ESI[†]), the first DRT dinuclear boron complex reported so far with a Ta-Ta dimer coordinated inside. It can also be viewed as a stack of two singlet $C_{9v} \text{Ta} \odot \text{B}_9^{2-}$ (1) or triplet $C_{9v} \text{Ta} \odot \text{B}_9$ units.²⁹ As shown in its configuration energy spectrum in Fig. S1b (ESI[†]), $\text{Ta}_2 @ \text{B}_{18}$ (3) is the well-defined GM of the system with $\Delta E_{\text{gap}} = 2.93 \text{ eV}$ and $\nu_{\text{min}} = 172 \text{ cm}^{-1}$. It lies 0.24 eV and 0.16 eV lower than the second lowest-lying DRT isomer $C_{2v} \text{Ta}_2 @ \text{B}_{18}$ at the PBE0 and CCSD(T) levels, respectively. A nonagonal $D_{9d} \text{Ta}_2 @ \text{B}_{18}$ with two Ta atoms capping both the top and bottom B_9 rings appears to lie much higher in energy

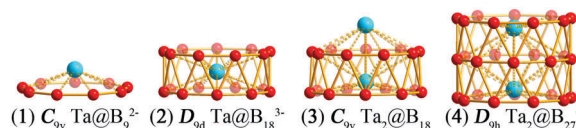


Fig. 1 Optimized structures of $\text{Ta} \odot \text{B}_9^{2-}$ (1), $\text{Ta} @ \text{B}_{18}^{3-}$ (2), $\text{Ta}_2 @ \text{B}_{18}$ (3), and $\text{Ta}_2 @ \text{B}_{27}^+$ (4) at the PBE0 level. Ta atoms are labelled in blue and B atoms in red.

than the GM (by 3.05 eV). Such a relative stability order is well reproduced at both the TPSSH and HSE06 levels (Fig. S2b, ESI†). $\text{Ta}_2@B_{18}$ (3) contains two non-equivalent Ta centers with the Ta-Ta bond length of $r_{\text{Ta-Ta}} = 2.37$ Å and bond order of $\text{WBI}_{\text{Ta-Ta}} = 1.37$, with one Ta atom lying 1.14 Å above the B_9 ring on the top and the other Ta coordinated inside the $C_{9v} B_{18}$ ligand 0.42 Å above the bottom B_9 ring, similar to the recently observed Nb-capped hexagonal antiprism $C_{6v} \text{Nb}_2\text{Si}_{12}$.⁵⁹ The Ta-Ta distance in 3 is about 0.1 Å longer than the Ta-Ta bond length of $r_{\text{Ta-Ta}} = 2.27$ Å in the quintet ground state of the Ta_2 dimer ($^5\Sigma_u$) at the same theoretical level. The top Ta atom possesses the Ta-B coordination distance of $r_{\text{Ta-B}} = 2.55$ Å and bond order of $\text{WBI}_{\text{Ta-B}} = 0.29$, while the bottom Ta has two different coordination distances with $r_{\text{Ta-B}} = 2.41/2.59$ Å and $\text{WBI}_{\text{Ta-B}} = 0.28/0.21$, respectively. They possess the electronic configurations of $\text{Ta}[\text{Xe}]5d^{0.13}6s^{3.92}$ and $\text{Ta}[\text{Xe}]5d^{0.24}6s^{4.11}$, total bond orders of $\text{WBI}_{\text{Ta}} = 4.75$ and 5.67, and natural atomic charges of $q_{\text{Ta}} = +0.92$ and $+0.42$ |e|, respectively (Table S1, ESI†). The bottom Ta center is more strongly coordinated to the DRT B_{18} ligand than the top Ta. $\text{Ta}_2@B_{18}$ (3) is predicted to have the vertical ionization potential of $\text{IP} = 6.91$ eV and electron affinity of $\text{EA} = 1.83$ eV at the PBE0 level.

Capping one more B_9 mono-ring atop $\text{Ta}_2@B_{18}$ (3) along the C_9 molecular axis generates the perfect TRT $D_{9h} \text{Ta}_2@B_{27}^+$ (4), which contains a Ta-Ta dimer coordinated inside a $D_{9h} B_{27}^+$ ligand with three staggered B_9 rings (Fig. S1c and S2c, ESI†), with $\Delta E_{\text{gap}} = 2.75$ eV and $\nu_{\text{min}} = 194$ cm^{-1} at the PBE0 level. It can be viewed as a stack of two singlet $C_{9v} \text{Ta} \odot B_9^{2-}$ (1) or two triplet $C_{9v} \text{Ta} \odot B_9$ units²⁹ with a B_9 middle deck sandwiched in between. It can also be constructed by coordinating a Ta-Ta dimer inside the previously predicted TRT $D_{9h} B_{27}^+$ cluster⁶⁰ with the Ta-Ta bond length of $r_{\text{Ta-Ta}} = 2.52$ Å (Table S1, ESI†). We notice that the Ta-Ta distance in 4 lies within the bond length range of 2.497–2.84 Å in the experimentally observed $\text{Ta}_2B_n^-$ ($n = 2-5$), which contains a Ta-Ta dimer surrounded by an incomplete boron equatorial belt.³³ As indicated in the configuration energy spectrum of $\text{Ta}_2B_{27}^+$ in Fig. S1c (ESI†), $\text{Ta}_2@B_{27}^+$ (4) is 0.28 eV more stable than the second lowest-lying cage-like isomer $C_1 \text{Ta}_2B_{27}^+$ and 0.90 eV more stable than its triplet TRT counterpart $C_{2v} \text{Ta}_2@B_{27}^+$ at the PBE0 level. Both TPSSH and HSE06 methods support the PBE0 relative energies well (Fig. S2c, ESI†). $\text{Ta}_2@B_{27}^+$ (4) possesses the optimized diameter of $d = 4.74$ Å and bond order of $\text{WBI}_{\text{Ta-Ta}} = 0.88$, Ta-B distance of $r_{\text{Ta-B}} = 2.40$ Å and bond order of $\text{WBI}_{\text{Ta-B}} = 0.33$ both on the top and at the bottom, and $r_{\text{Ta-B}} = 2.69$ Å and $\text{WBI}_{\text{Ta-B}} = 0.15$ between the Ta centers and the B_9 ring in the middle. The two equivalent Ta centers possess the electronic configuration of $\text{Ta}[\text{Xe}]5d^{4.26}6s^{0.21}$, total bond order of $\text{WBI} = 5.62$, and natural atomic charge of $q_{\text{Ta}} = +0.34$ |e| (Table S1, ESI†). These results are well comparable with the corresponding calculated values of the previously observed $\text{Ta}_2B_n^-$ ($n = 2-5$),³³ $\text{Ta} \odot B_n^-$ ($n = 9$ and 10),²² and $\text{Ta} @ B_{20}^-$,²⁵ indicating that effective Ta-Ta covalent bonding and $\text{Ta}_2-B_{27}^+$ coordination interactions exist in $\text{Ta}_2@B_{27}^+$ (4). Substituting Ta in $\text{Ta}_2@B_{27}^+$ (4) with its close neighbours in the periodic table produces TRT $D_{9h} \text{Nb}_2@B_{27}^+$, $D_{9h} \text{V}_2@B_{27}^+$, and $D_{9h} \text{Hf}_2@B_{27}^-$ isovalent with

$\text{Ta}_2@B_{27}^+$ (4), which are all true minima of the systems (Fig. S3, ESI†). Such monocations and monoanions may be produced and characterized in the gas phase in infrared photodissociation^{61,62} or PES³⁻¹⁰ measurements. Interestingly, in comparison with $\text{Ta}_2@B_{27}^+$ (4), a thinner TRT $D_{8h} \text{Cr}_2@B_{24}$ with three staggered B_8 rings in a $D_{8h} B_{24}$ ligand and a thicker TRT $D_{2h} \text{Zr}_2@B_{30}^{2+}$ with three staggered B_{10} rings in a $D_{2h} B_{30}$ ligand (Fig. S4, ESI†) also appear to be true GMs of the systems with $r_{\text{Cr-Cr}} = 2.10$ Å and $r_{\text{Zr-Zr}} = 3.19$ Å, $\text{WBI}_{\text{Cr}} = 5.75$ and $\text{WBI}_{\text{Zr}} = 4.20$, and $q_{\text{Cr}} = -0.34$ |e| and $q_{\text{Zr}} = +1.05$ |e|, respectively. It was noticed that two opposite hexacoordinate B atoms in the middle ring in TRT $D_{2h} \text{Zr}_2@B_{30}^{2+}$ are directly bound to two Ta centers on the top and at the bottom to form a $B_2\text{Ta}_2$ rhombus (Fig. S4, ESI†). The distorted $D_{2h} \text{Zr}_2@B_{30}^{2+}$ appears to be 0.39 eV more stable than a perfect TRT $D_{9h} \text{Zr}_2@B_{30}^{2+}$, indicating that a Zr-Zr dimer mismatches a TRT B_{30} ligand in the geometry.

The Ta-Ta dimer in $\text{Ta}_2@B_{27}^+$ (4) can be extended to a Ta-Ta-Ta trimer in penta-ring tubular (PRT) $D_{3h} \text{Ta}_3@B_{42}^-$ (Fig. S5, ESI†), which is a true minimum of the monoanion with $\Delta E_{\text{gap}} = 1.91$ eV and $\nu_{\text{min}} = 65$ cm^{-1} at the PBE0 level. Such a trinuclear PRT monoanion can be wrapped up from the observed most stable boron α -sheet on a Ag(111) substrate¹⁸⁻²⁰ with three hexagonal holes evenly distributed on the middle ring. Slightly distorted TRT $C_{3v} \text{Ta}_3@B_{42}^+$ and perfect $D_{3h} \text{Hf}_3@B_{42}$ similar to $D_{3h} \text{Ta}_3@B_{42}^-$ have also been obtained (Fig. S5, ESI†).

The PRT complexes can be further extended to form a 1D metalloboronanotube $\alpha\text{-Ta}_3@B_{48(3,0)}$ (5), which has P31M (C_{3v}) symmetry with an infinite -Ta-Ta- wire coordinated inside, as shown in Fig. 2a. With the optimized lattice parameter of $c = 8.75$ Å, average diameter of $d = 4.84$ Å, and average Ta-Ta distance of $r_{\text{Ta-Ta}} = 2.92$ Å, $\alpha\text{-Ta}_3@B_{48(3,0)}$ (5) is the thinnest arm-chair α -metalloboronanotube with a hole-density of $\eta = 1/9$ that can be wrapped up from the recently experimentally observed most stable free-standing boron α -sheet deposited on an Ag(111) substrate.¹⁸⁻²⁰ It possesses three hexacoordinate B atoms slightly buckled inwards and three hexacoordinate B atoms slightly bulked outwards around the C_3 axis in each C_{3v} unit cell. Interestingly, as shown in its calculated band structure in Fig. 2b, with a few bands crossing the Fermi level, $\alpha\text{-Ta}_3@B_{48(3,0)}$ (5) is predicted to be typically metallic in nature, in strong contrast to the slightly bulked pristine (3,0) α -boronanotube, which is a semiconductor with the band gap of $E_{\text{gap}} = 0.70$ eV at GGA.⁶³ The semiconductor-metal transition is induced by the strong hybridization coordination interactions between the B

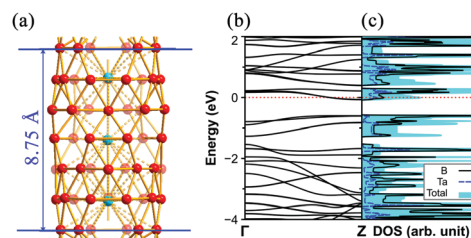


Fig. 2 Optimized (a) geometry, (b) band structure, and (c) density of states (DOS) of 1D metalloboronanotube $\alpha\text{-Ta}_3@B_{48(3,0)}$ (5) with P31M (C_{3v}) symmetry at the PBE level, with the lattice parameter c in the z direction indicated.

and Ta atoms in 1D α -Ta₃@B_{48(3,0)} (5) rather than from the impurity levels of the -Ta-Ta- wire coordinated inside, as shown in its density of states (DOS) in Fig. 2c in which the B atoms possess a slightly higher DOS value at the Fermi level than the Ta atoms in the system.

3.2 Bonding analyses and tubular aromaticity

To understand the high stability of these tubular species, we performed detailed AdNDP bonding analyses on them. As shown in Fig. 3a, mononuclear Ta@B₁₈³⁻ (2) possesses 18 3c-2e σ bonds on 18 B₃ triangles with the occupation number of ON = 1.94 |e| (ON values represent the number of electrons involved in the formation of a chemical bond, the ideal value is ON = 2) and 5 18c-2e σ bonds on the B₁₈ ligand with ON = 1.77-1.99 |e|. Over the C_{9v} σ -skeleton, there exist 3 18c-2e delocalized π bonds with ON = 1.69-1.99 |e|. The remaining 9 localized or delocalized bonds all involve the Ta-Ta dimer with ON = 1.98-2.00 |e|, including the 1 2c-2c σ bond (d_{z2}-d_{z2} overlap) on the Ta-Ta dimer along the C₉ molecular axis, 2 11c-2e π bonds between the Ta-Ta dimer and the B₉ ring at the bottom (d_{xz}- π and d_{yz}- π overlaps), 2 11c-2e π bonds between the Ta-Ta dimer and the B₉ ring on the top (d_{xz}- π and d_{yz}- π overlaps), and 4 20c-2e π bonds (d_{xy}- π and d_{x2-y2}- π overlaps) between Ta-Ta and the DRT B₁₈ ligand. In such a $\sigma + \pi$ double delocalization bonding pattern, each Ta center in Ta₂@B₁₈ (3) participates in 9 bonding interactions and conforms to the 18-electron configuration, rendering high thermodynamic stability to the neutral dinuclear complex.

With one more Ta center atop the B₁₈ ligand along the C₉ molecular axis, DRT Ta₂@B₁₈ (3) as a dinuclear complex inherits the main bonding characteristics of Ta@B₁₈³⁻ (2), with one more d_{z2}-d_{z2} σ bond formed on the Ta-Ta dimer (Fig. 3b). It possesses 18 3c-2e σ bonds on 18 B₃ triangles with ON = 1.93 |e| and 2 18c-2e σ bonds on the B₁₈ ligand with ON = 1.95 |e|. Over the C_{9v} σ -skeleton, there exist 3 18c-2e delocalized π bonds with ON = 1.69-1.99 |e|. The remaining 9 localized or delocalized bonds all involve the Ta-Ta dimer with ON = 1.98-2.00 |e|, including the 1 2c-2c σ bond (d_{z2}-d_{z2} overlap) on the Ta-Ta dimer along the C₉ molecular axis, 2 11c-2e π bonds between the Ta-Ta dimer and the B₉ ring at the bottom (d_{xz}- π and d_{yz}- π overlaps), 2 11c-2e π bonds between the Ta-Ta dimer and the B₉ ring on the top (d_{xz}- π and d_{yz}- π overlaps), and 4 20c-2e π bonds (d_{xy}- π and d_{x2-y2}- π overlaps) between Ta-Ta and the DRT B₁₈ ligand. In such a $\sigma + \pi$ double delocalization bonding pattern, each Ta center in Ta₂@B₁₈ (3) participates in 9 bonding interactions and conforms to the 18-electron configuration, rendering high thermodynamic stability to the neutral dinuclear complex.

With one more B₉ ring added in along the C₉ axis, Ta₂@B₂₇⁺ (4) as the first dinuclear TRT complex reported to date possesses 18 3c-2e σ bonds on 18 B₃ triangles with ON = 1.92 |e|, 9 4c-2e σ bonds on 9 B₄ rhombuses with ON = 1.91 |e|, and 5 27c-2e σ bonds with ON = 1.86-2.00 |e| on the B₂₇⁺ ligand (Fig. 3c). Over the D_{3h} σ -skeleton, there exist 2 27-2e delocalized π bonds on the B₂₇ ligand with ON = 1.65 |e| and 1.62 |e|, respectively. The remaining 11 bonds over the σ -skeleton all turn out to be effective coordination interactions involving the Ta-Ta dimer, including 1 11c-2e π bond between Ta-Ta and the B₉ middle ring mainly originating from the Ta-Ta d_{z2}-d_{z2} σ -overlap at the center (~74%) with ON = 1.90 |e|, 2 11c-2e π coordination bonds between Ta-Ta and the B₉ middle ring (d_{xz}- π and d_{yz}- π interactions) with ON = 1.77 |e|, 2 10c-2e π coordination bonds (d_{xz}- π and d_{yz}- π interactions) between the Ta center and the B₉ ring at the bottom and 2 10c-2e π coordination bonds (d_{xz}- π and d_{yz}- π) between the Ta center and the B₉ ring on the top with NO = 1.92 |e|, and 4 29c-2e π coordination bonds (d_{xy}- π and d_{x2-y2}- π overlaps) totally delocalized over the whole molecule with ON = 2.00 |e|. In such a bonding pattern, both the Ta centers in Ta₂@B₂₇⁺ (1) participate in 9 delocalized bonding interactions and match the 18-electron configuration in stable transition-metal complexes such as in the well-known 18-electron ferrocene Fe(C₅H₅)₂ and bis(benzene)chromium Cr(C₆H₆)₂. As shown in Fig. S6 (ESI[†]), similar $\sigma + \pi$ double delocalization bonding patterns exist in both the TRT D_{8h} Cr₂@B₂₄ and TRT D_{2h} Zr₂@B₃₀²⁺ in which both Cr and Zr centers possess 18-electron configurations. Such tubular dinuclear complexes behave like a molecular drum with two interconnected superatoms in 18-electron configurations at two ends. The $\sigma + \pi$ double delocalization bonding pattern revealed above renders tubular aromaticity to the TRT complexes, as evidenced by the calculated negative independent

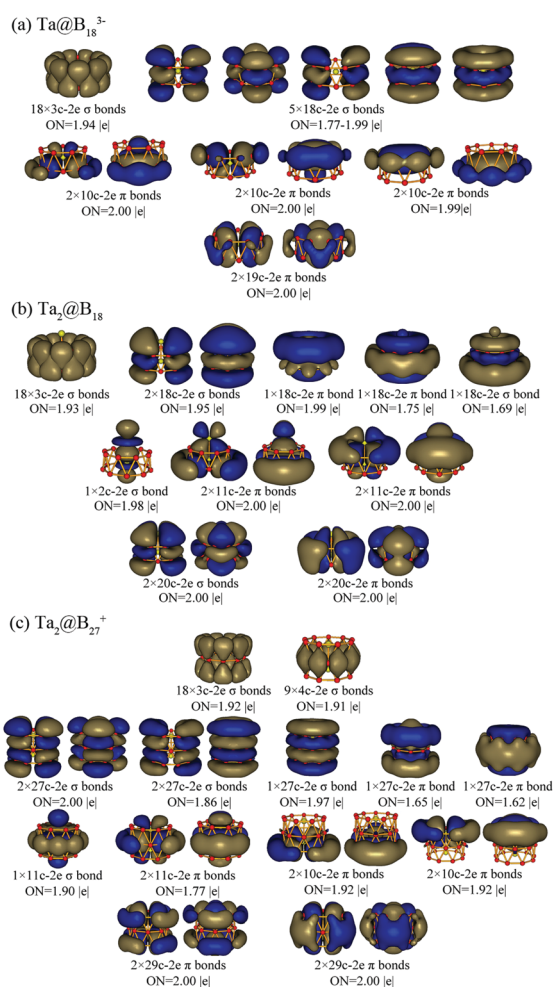


Fig. 3 AdNDP bonding patterns of (a) Ta@B₁₈³⁻ (2), (b) Ta₂@B₁₈ (3), and (c) Ta₂@B₂₇⁺ (4), with the occupation numbers (ONs) indicated.

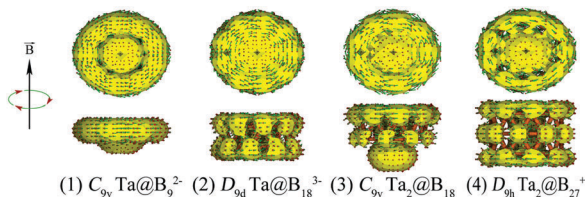


Fig. 4 Top and side views of the $\sigma + \pi$ ring current maps of **1–4** with an isosurface value of 0.05. The external magnetic field B is applied in the vertical direction parallel to the C_9 molecular axis, with the induced current vectors represented by red arrows on the isosurfaces.

nucleus chemical shifts of NICS = -98 ppm at the tube center and NICS = -46 ppm 1.0 \AA above the Ta atom in $\text{Ta}_2@B_{27}^+$ (**4**).

To further explore the aromatic nature of the concerned complexes, we plot the $\sigma + \pi$ ring current maps^{50,51} of **1–4** employing the prevalently used ACID approach^{50,51} in Fig. 4, with the corresponding ring current maps derived from the contributions of the delocalized σ electrons and the delocalized π electrons depicted in Fig. S7a and b (ESI[†]), respectively. Consistent magnetic responses occur in **1–4** in an external magnetic field in the vertical direction parallel to the C_9 molecular axis, irrespective of the electron type, similar to the situation observed in bare DRT B_{20} ⁶⁴ and TRT B_{27}^+ ,⁶⁰ which are known to possess typical tubular aromaticities and high thermodynamic stabilities. Such diatropic ring currents strongly suggest the aromatic characteristics of these thermodynamically stable Ta-doped boron complexes.

It is also noticed that, as shown in Fig. S8 (ESI[†]), the five unoccupied out-of-surface π canonical molecular orbitals of the D_{9h} B_{27}^+ ligand (LUMO, LUMO+1/LUMO+1', and LUMO+4/LUMO+4') that originate from the partially filled B $2p_z$ atomic orbitals interact effectively with the partially filled valence shell orbitals of the two Ta centers [$5d^36s^2$] to form five occupied spd- π hybridized coordination interactions in D_{9h} $\text{Ta}_2@B_{27}^+$ (**4**) (HOMO/HOMO', HOMO-1/HOMO-1', and HOMO-4). Such hybridizations effectively help stabilize the TRT dinuclear complex.

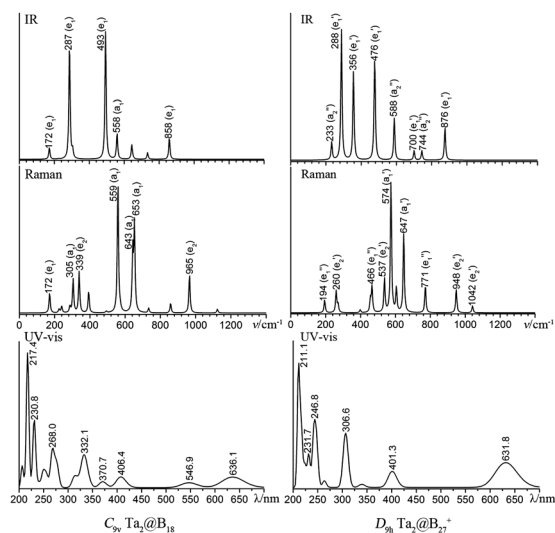


Fig. 5 Simulated IR, Raman, and UV-vis spectra of (a) $\text{Ta}_2@B_{18}$ (**3**) and (b) $\text{Ta}_2@B_{27}^+$ (**4**) in arbitrary relative intensities at the PBE0/6-311+G(d) level.

3.3 Simulated IR and Raman spectra

The infrared (IR), Raman, and UV-vis spectra of $\text{Ta}_2@B_{18}$ (**3**) and $\text{Ta}_2@B_{27}^+$ (**4**) were computationally simulated and are shown in Fig. 5 to facilitate their experimental characterization. Infrared photodissociation has been proven to be a powerful means to characterize novel clusters in gas phases.^{61,62} These high-symmetry tubular complexes possess relatively simple vibrational spectra with sharp features. Neutral $\text{Ta}_2@B_{18}$ (**3**) possesses two strong IR active peaks at $287 (e_1)$ and $498 (e_1) \text{ cm}^{-1}$ and two strong Raman active peaks at $558 (a_1)$ and $653 (a_1) \text{ cm}^{-1}$, which correspond to typical radial breathing modes (RBMs) of the tubular systems. The second Raman peak at 305 cm^{-1} mainly originates from a Ta-Ta stretching vibration (a_1) and the third peak at 339 cm^{-1} from a RBM mode (e_2) of the B_{18} ligand. Such RBMs may be used to characterize these tubular structures.⁶⁵ The strong UV bands around $217.4, 230.8, 268.0, 332.1,$ and 406.4 nm mainly originate from electronic transitions from deep inner shells of the neutral orbital to its high-lying unoccupied molecular orbitals, while the weak bands above 500 nm around 546.9 and 636.1 nm involve electronic excitations from the HOMO. As shown in Fig. 4b, $\text{Ta}_2@B_{27}^+$ (**4**) has similar spectral features to $\text{Ta}_2@B_{18}$ (**3**), with typical RBM vibrational modes at $260 (e_2')$, $574 (a_1')$, and $647 (a_1') \text{ cm}^{-1}$ in its Raman spectrum.

Conclusions

Based on extensive first-principles calculations, we have presented in this work the viable possibility of mononuclear DRT $\text{Ta}@B_{18}^{3-}$ (**2**) and dinuclear DRT $\text{Ta}_2@B_{18}$ (**3**) and TRT $\text{Ta}_2@B_{27}^+$ (**4**), which may be extended in a bottom-up approach to form the single-walled 1D α -boronanotube $\alpha\text{-Ta}_3@B_{48(3,0)}$ (**5**) with a transition-metal wire ($-\text{Ta}-\text{Ta}-$) coordinated inside. As the first tubular aromatic dinuclear boron complexes reported to date, DRT $\text{Ta}_2@B_{18}$ (**3**), TRT $\text{Ta}_2@B_{27}^+$ (**4**), TRT $\text{Cr}_2@B_{24}$, and TRT $\text{Zr}_2@B_{30}^{2+}$ with an effective $d_{z^2}-d_{z^2}$ M-M interaction along the main molecular axis turn out to follow the universal bonding pattern of $\sigma + \pi$ double delocalization with each transition-metal center conforming to the 18-electron rule, presenting a plausible mechanism to form metallic α -metalloboronanotubes with direct metal-metal interactions along the $-\text{M}-\text{M}-$ wire inside. Single- or multi-walled tubular multinuclear boron complexes and their cage-like rivals or core-shell conformers may compete in a wide range of cluster sizes to form a promising area in both chemistry and materials science.

Conflicts of interest

There are no conflicts to declare.

Acknowledgements

The work was supported by the National Natural Science Foundation of China (21720102006 to S.-D. Li, 2018BY001 to H.-R. Li, 11504213 to Y.-W. Mu, and 21473106 to H.-G. Lu).

Notes and references

- W. N. Lipscomb, *Science*, 1977, **196**, 1047.
- F. A. Cotton, G. Wilkinson, C. A. Murrillo and M. Bochmann, *Advanced inorganic chemistry*, Wiley, New York, 6th edn, 1999.
- L. S. Wang, *Int. Rev. Phys. Chem.*, 2016, **35**, 69–142.
- A. P. Sergeeva, I. A. Popov, Z. A. Piazza, W. L. Li, C. Romanescu, L. S. Wang and A. I. Boldyrev, *Acc. Chem. Res.*, 2014, **47**, 1349–1358.
- H. J. Zhai, Y. F. Zhao, W. L. Li, Q. Chen, H. Bai, H. S. Hu, Z. A. Piazza, W. J. Tian, H. G. Lu, Y. B. Wu, Y. W. Mu, G. F. Wei, Z. P. Liu, J. Li, S. D. Li and L. S. Wang, *Nat. Chem.*, 2014, **6**, 727–731.
- Q. Chen, W. L. Li, Y. F. Zhao, S. Y. Zhang, H. S. Hu, H. Bai, H. R. Li, W. J. Tian, H. G. Lu, H. J. Zhai, S. D. Li, J. Li and L. S. Wang, *ACS Nano*, 2015, **9**, 754–760.
- Y. J. Wang, Y. F. Zhao, W. L. Li, T. Jian, Q. Chen, X. R. You, T. Ou, X. Y. Zhao, H. J. Zhai, S. D. Li, J. Li and L. S. Wang, *J. Chem. Phys.*, 2016, **144**, 064307.
- H. R. Li, T. Jian, W. L. Li, C. Q. Miao, Y. J. Wang, Q. Chen, X. M. Luo, K. Wang, H. J. Zhai, S. D. Li and L. S. Wang, *Phys. Chem. Chem. Phys.*, 2016, **18**, 29147–29155.
- Q. Chen, W. L. Li, X. Y. Zhao, H. R. Li, L. Y. Feng, H. J. Zhai, S. D. Li and L. S. Wang, *Eur. J. Inorg. Chem.*, 2017, 4546–4551.
- Q. Chen, W. J. Tian, L. Y. Feng, H. G. Lu, Y. W. Mu, H. J. Zhai, S. D. Li and L. S. Wang, *Nanoscale*, 2017, **9**, 4550–4557.
- Q. Chen, S. Y. Zhang, H. Bai, W. J. Tian, T. Gao, H. R. Li, C. Q. Miao, Y. W. Mu, H. G. Lu, H. J. Zhai and S. D. Li, *Angew. Chem., Int. Ed.*, 2015, **54**, 8160–8164.
- Q. Chen, H. R. Li, C. Q. Miao, Y. J. Wang, H. G. Lu, Y. W. Mu, G. M. Ren, H. J. Zhai and S. D. Li, *Phys. Chem. Chem. Phys.*, 2016, **18**, 11610–11615.
- Q. Chen, H. R. Li, W. J. Tian, H. G. Lu, H. J. Zhai and S. D. Li, *Phys. Chem. Chem. Phys.*, 2016, **18**, 14186–14190.
- W. J. Tian, Q. Chen, H. R. Li, M. Yan, Y. W. Mu, H. G. Lu, H. J. Zhai and S. D. Li, *Phys. Chem. Chem. Phys.*, 2016, **18**, 9922–9926.
- E. Oger, N. R. Crawford, R. Kelting, P. Weis, M. M. Kappes and R. Ahlrichs, *Angew. Chem., Int. Ed.*, 2007, **46**, 8503–8506.
- D. Ciuparu, R. F. Klie, Y. M. Zhu and L. Pfeifferle, *J. Phys. Chem. B*, 2004, **108**, 3967–3969.
- F. Liu, C. Shen, Z. Su, X. Ding, S. Deng, J. Chen, N. Xu and H. Gao, *J. Mater. Chem.*, 2010, **20**, 2197–2205.
- X. Yang, Y. Ding and J. Ni, *Phys. Rev. B: Condens. Matter Mater. Phys.*, 2008, **77**, 041402.
- H. Tang and S. Ismail-Beigi, *Phys. Rev. Lett.*, 2007, **99**, 115501.
- Q. Zhong, J. Zhang, P. Cheng, B. Feng, W. Li, S. Sheng, H. Li, S. Meng, L. Chen and K. Wu, *J. Phys.: Condens. Matter*, 2017, **29**, 095002.
- R. R. Zope and T. Baruah, *Chem. Phys. Lett.*, 2011, **501**, 193–196.
- C. Romanescu, T. R. Galeev, W. L. Li, A. I. Boldyrev and L. S. Wang, *Acc. Chem. Res.*, 2013, **46**, 350–358.
- I. A. Popov, T. Jian, G. V. Lopez, A. I. Boldyrev and L. S. Wang, *Nat. Commun.*, 2015, **6**, 8654.
- T. Jian, W.-L. Li, X. Chen, T.-T. Chen, G. V. Lopez, J. Li and L. S. Wang, *Chem. Sci.*, 2016, **7**, 7020.
- W. L. Li, T. Jian, X. Chen, H. R. Li, T. T. Chen, X. M. Luo, S. D. Li, J. Li and L. S. Wang, *Chem. Commun.*, 2017, **53**, 1587–1590.
- X. Y. Zhao, X. M. Luo, X. X. Tian, H. G. Lu and S. D. Li, *J. Cluster Sci.*, 2018, to be published.
- H. R. Li, H. Liu, X. X. Tian, W. Y. Zan, Y. W. Mu, H. G. Lu, J. Li, Y. K. Wang and S. D. Li, *Phys. Chem. Chem. Phys.*, 2017, **19**, 27025–27030.
- H. R. Li, H. Liu, X. Q. Lu, W. Y. Zan, X. X. Tian, H. G. Lu, Y. B. Wu, Y. W. Mu and S. D. Li, *Nanoscale*, 2018, **10**, 7451.
- C. Romanescu, T. R. Galeev, W. L. Li, A. I. Boldyrev and L. S. Wang, *J. Chem. Phys.*, 2013, **138**, 134315.
- B. Le Chen, W. G. Sun, X. Y. Kuang, C. Lu, X. X. Xia, H. X. Shi and G. Maroulis, *Inorg. Chem.*, 2018, **57**, 343–350.
- H. Bai, Q. Chen, H. J. Zhai and S. D. Li, *Angew. Chem., Int. Ed.*, 2015, **54**, 941–945.
- W. J. Tian, Q. Chen, X. X. Tian, Y. W. Mu, H. G. Lu and S. D. Li, *Sci. Rep.*, 2016, **6**, 37893.
- L. Xie, W. L. Li, C. Romanescu, X. Huang and L. S. Wang, *J. Chem. Phys.*, 2013, **138**, 034308.
- H. R. Li, X. X. Tian, X. M. Luo, M. Yan, Y. W. Mu, H. G. Lu and S. D. Li, *Sci. Rep.*, 2017, **7**, 5701.
- S. Goedecker, *J. Chem. Phys.*, 2004, **120**, 9911.
- S. Goedecker, W. Hellmann and T. Lenosky, *Phys. Rev. Lett.*, 2005, **95**, 055501.
- X. Chen, Y. F. Zhao, L. S. Wang and J. Li, *Comput. Theor. Chem.*, 2017, **1107**, 57.
- C. Adamo and V. Barone, *J. Chem. Phys.*, 1999, **110**, 6158–6170.
- J. Tao, J. P. Perdew, V. N. Staroverov and G. E. Scuseria, *Phys. Rev. Lett.*, 2003, **91**, 146401.
- J. Heyd, G. E. Scuseria and M. Ernzerhof, *J. Chem. Phys.*, 2003, **118**, 8207–8215.
- R. Krishnan, J. S. Binkley, R. Seeger and J. A. Pople, *J. Chem. Phys.*, 1980, **72**, 650–654.
- D. Feller, *J. Comput. Chem.*, 1996, **17**, 1571–1586.
- K. L. Schuchardt, B. T. Didier, T. Elsethagen, L. Sun, V. Gurumoorathi, J. Chase, J. Li and T. L. Windus, *J. Chem. Inf. Model.*, 2007, **47**, 1045–1052.
- M. J. Frisch, *et al.*, *Gaussian 09 (Revision D.01)*, Gaussian Inc., Wallingford, CT, 2013.
- J. Čížek, *Adv. Chem. Phys.*, 1969, **14**, 35.
- G. D. Purvis III and R. J. Bartlett, *J. Chem. Phys.*, 1982, **76**, 1910–1918.
- K. Raghavachari, G. W. Trucks, J. A. Pople and M. Head-Gordon, *Chem. Phys. Lett.*, 1989, **157**, 479–483.
- H. J. Werner, *et al.*, *Molpro, version*, 2012.1 (www.molpro.net).
- D. Y. Zubarev and A. I. Boldyrev, *Phys. Chem. Chem. Phys.*, 2008, **10**, 5207.
- R. Herges and D. Geuenich, *J. Phys. Chem. A*, 2011, **105**, 3214–3220.
- D. Geuenich, K. Hess, F. Köhler and R. Herges, *Chem. Rev.*, 2005, **105**, 3758–3772.
- R. Bauernschmitt and R. Ahlrichs, *Chem. Phys. Lett.*, 1996, **256**, 454–464.
- P. E. D. Glendening, J. K. Badenhoop, A. E. Reed, J. E. Carpenter, J. A. Bohmann, C. M. Morales, C. R. Landis and F. Weinhold, *NBO 6.0*, 2013, <http://nbo6.chem.wisc.edu>.

- 54 G. Kresse and J. Furthmuller, *Phys. Rev. B: Condens. Matter Mater. Phys.*, 1996, **54**, 11169–11186.
- 55 G. Kresse and J. Hafner, *J. Phys.: Condens. Matter*, 1994, **6**, 8245–8257.
- 56 J. P. Perdew, K. Burke and M. Ernzerhof, *Phys. Rev. Lett.*, 1996, **77**, 3865–3868.
- 57 P. E. Blochl, *Phys. Rev. B: Condens. Matter Mater. Phys.*, 1994, **50**, 17953–17979.
- 58 G. Kresse and D. Joubert, *Phys. Rev. B: Condens. Matter Mater. Phys.*, 1999, **59**, 1758–1775.
- 59 S. J. Lu, H. G. Xu, X. L. Xu and W. J. Zheng, *J. Phys. Chem. C*, 2017, **121**, 11851–11861.
- 60 L. V. Duong, H. T. Pham, N. M. Tam and M. T. Nguyen, *Phys. Chem. Chem. Phys.*, 2014, **16**, 19470–19478.
- 61 G. Wang, M. Zhou, J. T. Goettel, G. J. Schrobilgen, J. Su, J. Li, T. Schloder and S. Riedel, *Nature*, 2014, **514**, 475–477.
- 62 M. R. Fagiani, X. W. Song, P. Petkov, S. Debnath, S. Gewinner, W. Schöllkopf, T. Heine, A. Fielicke and K. R. Asmis, *Angew. Chem., Int. Ed.*, 2016, **56**, 501–504.
- 63 H. Tang and S. Ismail-Beigi, *Phys. Rev. B: Condens. Matter Mater. Phys.*, 2010, **82**, 115412.
- 64 M. P. Johansson, *J. Phys. Chem. C*, 2009, **113**, 524–530.
- 65 D. Ciuparu, R. F. Klie, Y. M. Zhu and L. Pfefferle, *J. Phys. Chem. B*, 2004, **108**, 3967.